

# Effects of a local defect on one-dimensional nonlinear surface growth

Hyungjoon Soh,<sup>1</sup> Yongjoo Baek,<sup>2</sup> Meesoon Ha,<sup>3,\*</sup> and Hawoong Jeong<sup>4</sup>

<sup>1</sup>Department of Physics, Korea Advanced Institute of Science and Technology, Daejeon 34141, Korea

<sup>2</sup>Department of Physics, Technion-Israel Institute of Technology, Haifa 32000, Israel

<sup>3</sup>Department of Physics Education, Chosun University, Gwangju 61452, Korea

<sup>4</sup>Department of Physics and Institute for the BioCentury,  
Korea Advanced Institute of Science and Technology, Daejeon 34141, Korea

(Dated: November 15, 2016)

The slow-bond problem is a long-standing question about the minimal strength of a local defect with global effects on the Kardar–Parisi–Zhang (KPZ) universality class. A consensus on the issue has been delayed due to discrepancy between various analytical predictions and numerical observations. We revisit the problem from a numerical perspective, using the statistics of passive sliders driven by nonlinear surface growth as new measures of the slow-bond effects, in addition to more traditional observables like the steady-state current. For different observables and boundary conditions, we consistently identify a scaling relation which rules out the previously reported nonzero critical point but leaves open the possibility of an essential singularity at the vanishing critical strength of the slow bond.

PACS numbers: 02.50.-r, 05.40.-a, 64.60.-i, 64.60.Ht

## I. INTRODUCTION

The Kardar–Parisi–Zhang (KPZ) equation [1] for the one-dimensional (1D) case describes a broad range of nonequilibrium phenomena, such as nonlinear surface growth [2–4], biased transport of particles [5], fluctuations of directed polymers [3, 6], and so on. Being a rare example of nonequilibrium processes whose steady-state statistics are fully known, the KPZ equation has received much attention as the governing dynamics underlying a universality class beyond equilibrium [7, 8]. Recent experimental realizations of these statistics [9] have placed the KPZ universality class on a firm empirical basis.

In spite of these advances, open questions still remain. One important example is whether a *local* defect is relevant to macroscopic properties. Nonequilibrium systems with a conserved quantity generically display weak long-range correlations, even far away from criticality [10–12]. This opens up the possibility that even local perturbations may have global consequences in the presence of nonequilibrium driving; however, there is no known general criterion for determining how strong a local defect should be to induce such phenomena. For 1D systems governed by the KPZ equation, this issue gave rise to the *slow-bond* (or *blockage*) problem, which has been a subject of much debate.

Using the language of lattice gases, the slow-bond problem can be stated as follows [13]. Consider self-driven particles with excluded volume interactions hopping in one direction through a 1D lattice. If the hopping is slowed down by a factor of  $1 - \epsilon$  across one fixed bond (see Fig. 1), how *slow* should the bond be to create a queue of particles before it (or vacancies after it) on a

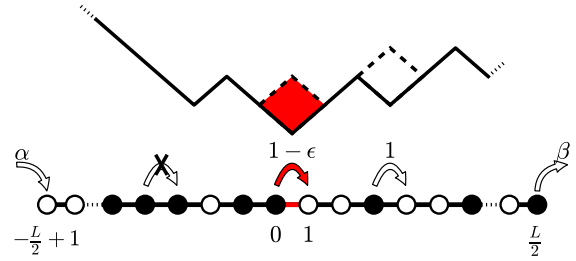


FIG. 1. 1D TASEP (lower) and the corresponding BCSOS growth model (upper) with a slow bond of strength  $\epsilon \in [0, 1]$  (marked by a red segment) and open boundaries. The numbers above the arrows indicate hopping rates, and the site indices are shown at the bottom.

macroscopic length scale? Two conflicting hypotheses have been proposed. On one side, a slow bond of any strength is claimed to have long-range effects (i.e., the critical strength is  $\epsilon_c = 0$ ). This claim is supported by approximate analytical arguments based on the mean-field theory [14, 15], series expansions with respect to small  $\epsilon$  [16, 17], and renormalization group arguments [18, 19]. On the other side, a weak slow-bond regime is claimed to exist (for  $0 < \epsilon < \epsilon_c$ ), in which the effects of the slow bond decays algebraically to zero with distance, yielding a *weakly-localized* queue (see Fig. 2). This hypothesis was put forth by [20] based on finite-size scaling of numerical results, with an estimate of  $\epsilon_c = 0.20(2)$ . Similar claims for  $\epsilon_c > 0$  can also be found in other numerical studies [21, 22] and notably in an experiment on the slow combustion of a paper with a columnar defect [23]. Due to the lack of exact analytical methods, the controversy has remained unresolved for more than a couple of decades [24].

More recently, [25] claimed to have rigorously proven  $\epsilon_c = 0$ , which necessitates reconsideration of the numeri-

\* Corresponding author: [msha@chosun.ac.kr](mailto:msha@chosun.ac.kr)

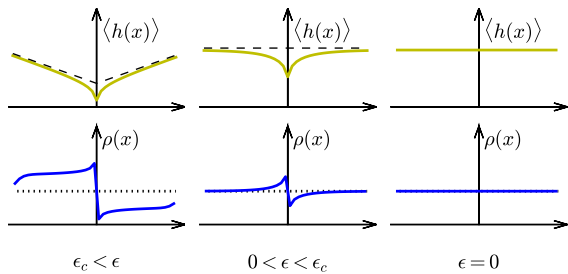


FIG. 2. Average height profiles of the BCSOS growth model (upper) and density profiles of the TASEP (lower) under the assumption of  $\epsilon_c > 0$ . In the strong slow-bond regime ( $\epsilon > \epsilon_c$ ), the TASEP (BCSOS growth model) develops a queue (valley) spanning the system. In the weak slow-bond regime ( $0 < \epsilon < \epsilon_c$ ), the queue (valley) becomes weakly localized around the slow bond. In the absence of the slow bond ( $\epsilon = 0$ ), the queue (valley) vanishes.

cal analyses claimed to support  $\epsilon_c > 0$ . An ensuing report on high-precision simulations [26] seems to indicate that  $\epsilon_c$  is at least much smaller than previously claimed, with some hallmarks of global slow-bond effects persistently detected down to  $\epsilon \geq 0.01$ . While these results are again in favor of  $\epsilon_c = 0$ , there are some subtle but important differences in the boundary conditions employed in different numerical studies (see Sec. II C for details). In order to address the seeming disagreement between the studies more thoroughly, we should check whether consistent observations can be made irrespective of the boundary conditions. Moreover, it would be informative to analyze the numerical results in terms of new physical observables and check whether consistent observations can be made.

In this paper, we revisit the slow-bond problem via extensive Monte Carlo simulations for both open and closed boundary conditions. While previous studies have been limited to observations of the steady-state current and the density profile, we propose a new observable reflecting the effects of a slow bond, namely the passive slider statistics. Passive sliders, which include positive (advected) and negative (anti-advected) sliders [27], are driven in a certain direction whenever there is a contiguous queue of particles or vacancies; thus their dynamics provide a convenient means of detecting the range of a queue created by a slow bond. Our numerical analysis shows that both the conventional current statistics and the new passive slider statistics exhibit the exponential scaling form suggested by [17], which is a characteristic of an essential singularity at  $\epsilon_c = 0$ . Although our results are not a definite proof of  $\epsilon_c = 0$ , they do rule out  $\epsilon_c = 0.20(2)$  and the associated power-law behaviors previously reported in [20].

The rest of the paper is organized as follows. In Sec. II, we first introduce the slow-bond problem and its representations in two simplest examples of the KPZ universal class, namely the totally asymmetric simple exclusion

process (TASEP) and the body-centered solid-on-solid (BCSOS) model of surface growth. In Sec. III, we focus on the finite-size effects associated with the steady-state current. Implications of the passive slider statistics are discussed in Sec. IV. Finally, a summary of our results is given in Sec. V.

## II. MODELS AND PROBLEMS

### A. TASEP with a slow bond

One of the simplest lattice gas models belonging to the KPZ universality class is the totally asymmetric simple exclusion process (TASEP). Here we present a standard discrete-time implementation of the model in the presence of a slow bond.

We consider a 1D lattice with  $L$  sites. For convenience,  $L$  is assumed to be an even number, so that the sites can be indexed by  $x = -L/2 + 1, \dots, 0, \dots, L/2$ . Each site can be occupied by at most a single particle, so that the occupancy of site  $x$  satisfies  $n(x) \in \{0, 1\}$ . At each time step, a randomly chosen bond is updated by

$$\bullet \circ \longrightarrow \circ \bullet \quad (1)$$

if and only if the left end of the bond is occupied ( $\bullet$ ) and the right end is vacant ( $\circ$ ). The only exception to this rule is that, for the bond between sites 0 and 1, the above update takes place with probability  $1 - \epsilon$  with  $\epsilon \geq 0$ . Thus the bond between sites 0 and 1 is our slow bond.

There are two possible boundary conditions for the system. For the periodic boundary condition (PBC), the leftmost site  $-L/2 + 1$  is adjacent to rightmost site  $L/2$ , so that the system forms a closed loop. Since the number of particles is fixed (say at  $N \leq L$ ), the density of particles  $\rho_0 \equiv N/L$  can be regarded as the control parameter. On the other hand, for the open boundary condition (OBC), each end of the system is connected by a bond to its own particle reservoir (see Fig. 1). If the bond between the left (right) reservoir and site  $-L/2 + 1$  ( $L/2$ ) is chosen, provided that the site is vacant (occupied), a particle jumps into (out of) the site with probability  $\alpha$  ( $\beta$ ). Note that for the OBC the slow bond is exactly in the middle of the system. For reasons to be explained later (see Sec. II C), we choose  $\rho_0 = 1/2$  for the PBC and  $\alpha = \beta = 1/2$  for the OBC.

In order to implement the continuous flow of time, after each step the time is increased by

$$t \longrightarrow t + \frac{\ln(1/u)}{\text{number of bonds}}, \quad (2)$$

where  $u \in [0, 1)$  is a uniformly distributed random number. This ensures that each bond is chosen by a Poisson process of rate 1. Since the fluctuations of the Poisson process are irrelevant to the observed steady-state statistics, we can reduce the computational cost without affecting the results by replacing  $\ln(1/u)$  with 1, so that the

time is updated deterministically. Even then the number of bonds in the denominator sets the correct time scale for our simulation.

To make our discussions self-contained, we give a brief account of the dynamical phases of the TASEP in the limit  $L \rightarrow \infty$  for  $\epsilon = 0$ , which can be described by both mean-field approximations and exact methods (see [5] and references therein). In the steady state, the system develops a bulk region in which the average density of particles forms a flat profile  $\rho(x) \equiv \langle n(x) \rangle = \rho_b$ , where  $\langle \cdot \rangle$  denotes an ensemble average. Since correlations between adjacent sites become zero in this region, the steady-state current  $J$ , defined as the average number of particles hopping through each bond per unit time, is related to the bulk density  $\rho_b$  by

$$J = \langle n(x) [1 - n(x+1)] \rangle = \rho(x) [1 - \rho(x+1)] = \rho_b(1 - \rho_b). \quad (3)$$

For the PBC, we always have a flat average density profile throughout the system, so  $\rho_b = \rho_0$  and  $J = \rho_0(1 - \rho_0)$ . In this case the maximal-current phase, characterized by  $J = 1/4$  and  $\rho_b = 1/2$ , is attained only at  $\rho_0 = 1/2$ ; otherwise, for  $\rho_0 < 1/2$  ( $\rho_0 > 1/2$ ) the system is in the low-density (high-density) phase characterized by excess hole (particle) density in the bulk.

On the other hand, for the OBC the bulk density is given by

$$\rho_b = \begin{cases} \min[\alpha, 1/2] & \text{if } \alpha \leq \beta; \\ \max[1 - \beta, 1/2] & \text{otherwise.} \end{cases} \quad (4)$$

In this case the maximal current  $J = 1/4$  is attained only for  $\alpha \geq 1/2$  and  $\beta \geq 1/2$ ; otherwise, the system is in the low-density (high-density) phase for  $\alpha < \beta$  ( $\alpha > \beta$ ), in which the bulk density  $\rho_b$  is controlled by the entry rate  $\alpha$  (exit rate  $\beta$ ). If  $\alpha = \beta < 1/2$ , the system exhibits a phase separation into a pair of low-density and high-density regions, with a sharp interface (called *shock*) formed between the two.

### B. Mapping to surface growth

It is often useful to reinterpret the TASEP in terms of a related surface growth process called the body-centered solid-on-solid (BCSOS) growth model [28]. The mapping from a particle configuration of the TASEP to a height profile of the BCSOS growth model is simply given by the relation

$$h(x) \equiv h\left(-\frac{L-1}{2}\right) + \sum_{y=-\frac{L}{2}+1}^{x-\frac{1}{2}} [1 - 2n(y)] \quad (5)$$

for  $x = -\frac{L-3}{2}, -\frac{L-5}{2}, \dots, \frac{L+1}{2}$  (see Fig. 1). This implies that the height difference between adjacent sites is always  $\Delta h = \pm 1$  and that a hopping from site  $x$  to site  $x+1$

corresponds to the deposition  $h(x + \frac{1}{2}) \rightarrow h(x + \frac{1}{2}) + 2$  (see the tilted blocks with dashed boundaries in Fig. 1). Similarly, each entry from the left reservoir (exit to the right reservoir) corresponds to an increase of the height at  $x = -\frac{L-1}{2}$  ( $x = \frac{L+1}{2}$ ) by two. Due to the slow bond, the deposition also slows down by a factor of  $1 - \epsilon$  at  $x = \frac{1}{2}$ .

### C. Slow-bond problem

With two simple implementations of the KPZ universality class introduced above, we now give a precise formulation of the slow-bond problem in terms of these models. We consider the case when the system is, if there is no slow bond ( $\epsilon = 0$ ), in the maximal-current phase ( $J = 1/4$ ,  $\rho_b = 1/2$ ). This means that the control parameters should be given by  $\rho_0 = 1/2$  for the PBC and  $\alpha \geq 1/2$ ,  $\beta \geq 1/2$  for the OBC. We note that  $\alpha = \beta = 1$  was used in [26], which puts the system deep inside the maximal-current regime to avoid possible complications near the phase boundary. On the other hand,  $\alpha = \beta = 1/2$  was used in [20], with the purpose of flattening the density profile near the the reservoirs when the bulk density satisfies  $\rho_b = 1/2$ . This ensures that, in the claimed weak slow-bond regime, a localized queue around the slow bond becomes easier to observe. In this study, we use the latter condition for a closer comparison with [20]. Once the control parameters are thus fixed, the slow-bond strength  $\epsilon$  becomes the only free parameter.

The critical strength  $\epsilon_c$  of the slow bond is defined as follows. If  $0 \leq \epsilon \leq \epsilon_c$ , the steady-state current remains at its maximal value  $J = 1/4$ . Equivalently, the bulk density before and after the slow bond is given by its maximal-current value  $\rho_b = 1/2$ . In the language of the BCSOS growth model, the average height profile  $\langle h(x) \rangle$  remains largely flat before and after the slow bond.

On the other hand, if  $\epsilon > \epsilon_c$ ,  $J$  becomes smaller than  $1/4$ , which is equivalent to an increase (decrease) of  $\rho_b$  from  $1/2$  before (after) the slow bond. We may denote the change of the bulk density by

$$\Delta_b(\epsilon) \equiv \rho_b(\epsilon) - \rho_b \quad (6)$$

and use it as an indicator of whether a macroscopic queue is formed around the slow bond. We note that  $-\Delta_b$  can also be interpreted as the average slope of the height profile in the BCSOS growth model.

The slow-bond problem is a question on the precise value of  $\epsilon_c$ . In Fig. 2, under the assumption that  $\epsilon_c > 0$  according to the scenario proposed by [20], we give schematic illustrations of the height profiles of the BCSOS growth model (upper panel) and the density profiles of the TASEP (lower panel). Boundaries at the slow bond, reservoirs (for the OBC), or between high-density and low-density regions (for the PBC) generally produce some nonlinear modulations, which gradually decay as one moves away from the boundaries into the bulk. If the weak slow-bond regime  $0 < \epsilon < \epsilon_c$  exists, it can be

distinguished from the case  $\epsilon = 0$  by such density (or height) modulations near the slow bond (see the middle column of Fig. 2). It was claimed in [20] that these boundary effects show a power-law decay and thus are only weakly localized. On the other hand, if  $\epsilon_c = 0$ , the weak slow-bond regime would simply be nonexistent.

Based on these scenarios, we aim to estimate the value of  $\epsilon_c$  for both PBC and OBC by extensive Monte Carlo simulations.

#### D. Simulation method

For any boundary condition, we start each run of the simulation from the initial condition in which one particle is occupying every second site (“•◦•◦•◦•”). For the PBC, this initial condition automatically sets  $\rho_0 = 1/2$ . As long as  $\rho_0$  is correctly set (for the PBC) and the simulation time is sufficiently longer than the relaxation time, the precise form of the initial condition is irrelevant to the results. Assuming that the decay time for any correlation in the system grows as  $L^{3/2}$  (KPZ scaling) or slower, we let the system evolve until  $t = 100L^{3/2}$  in order to ensure that the system reaches the steady state. After then we measure the observables of interest at every  $L^{3/2}$  time steps, so that all measurements can be regarded as independent of each other.

In order to reduce the simulation time, we keep a list of “active bonds”, which are bonds with the right configuration (“•◦”) for a hopping to occur. The bond connecting the leftmost (rightmost) site to the adjacent reservoir is also included in the list if the site is vacant (occupied). At each step, one of the bonds in the list is chosen at random and updated according to the rules of the process. This method decreases the number of random number generations [29] required for each hopping to occur. Instead, each update should increase the time by

$$t \longrightarrow t + \frac{\ln(1/u)}{\text{number of active bonds}}, \quad (7)$$

where  $u \in [0, 1]$  is a uniformly distributed random number. As previously discussed,  $\ln(1/u)$  can be replaced with 1 for convenience. This scheme increases the time faster than Eq. (2) does.

### III. STEADY-STATE CURRENT

As explained in Sec. II C, one of the observables directly indicating the effects of a slow bond is the steady-state current  $J$ . In this section, we present numerical results on how  $J$  depends on the slow-bond strength  $\epsilon$  and the system size  $L$ . The central quantity of interest is

$$\Delta_J(\epsilon; L) \equiv J(0; L) - J(\epsilon; L). \quad (8)$$

Here  $J(\epsilon; L)$  denotes the numerically measured value of the steady-state current for the given values of  $\epsilon \in (0, 1]$

and  $L$ . The value of  $J(0; L)$  can be calculated exactly:  $J(0; L) = 1/4$  for the OBC with  $\alpha = \beta = 1/2$  [30], and  $J(0; L) = \frac{1}{4(1-1/L)}$  for the PBC with  $\rho_0 = 1/2$  [5]. One can easily verify these values of  $J(0; L)$  by numerics. That said, the quantity  $\Delta_J(\epsilon; L)$  indicates the observed change of the current due to the slow bond at finite system size. Some analytical studies [16, 17] argued that in the limit  $L \rightarrow \infty$  this quantity obeys the relation

$$\Delta_J \sim \exp(-b/\epsilon), \quad (9)$$

where  $b \simeq 2$  according to [17]. If true, this relation supports  $\epsilon_c = 0$  and confirms the existence of an essential singularity at the transition point, which was predicted by renormalization group arguments [18, 19]. In what follows we numerically check the plausibility of Eq. (9).

Figure 3 shows the behaviors of the steady-state current as a function of  $\epsilon$  and  $L$ , where the upper panel shows the results for the OBC with  $\alpha = \beta = 1/2$ . As shown in Fig. 3(a), the steady-state current  $J$  monotonically increases towards the maximal value  $1/4$  as the slow-bond strength  $\epsilon$  is decreased. This is consistent with the intuition that  $\Delta_J$  must be a monotonically increasing function of  $\epsilon$ . For  $\epsilon$  larger than 0.2,  $\Delta_J$  closely follows the exponential form shown in Eq. (9), as shown by the black solid lines in Fig. 3(b). By the method of least squares, we obtain an estimation  $b \simeq 2.24$ , which is slightly higher than  $b \simeq 2$  suggested by [17] (see the blue solid lines in Fig. 3 for comparison). Since Eq. (9) describes the leading-order behavior in the limit  $\epsilon \rightarrow 0$ , this deviation seems to be a systematic bias due to higher-order contributions in  $\epsilon$ . Taking this bias into account, the result seems consistent with the vanishing critical point  $\epsilon_c = 0$ .

For values of  $\epsilon$  smaller than 0.2, the agreement with Eq. (9) becomes poor due to the effects of finite  $L$ . Still, we observe that  $\Delta_J$  stays greater than the values predicted by Eq. (9). This is again in favor with  $\epsilon_c = 0$ . Since  $\Delta_J$  decreases with  $L$ , one may ask whether  $\Delta_J$  could eventually go below the exponential curve of Eq. (9), so that  $\epsilon_c > 0$  is still possible. According to Fig. 3(c), the decay with  $L$  seems to be ranging between a  $1/L$  scaling and saturation. Assuming that the  $1/L$  decay continues, one may estimate  $\lim_{L \rightarrow \infty} \Delta_J(\epsilon; L)$  by fitting the data obtained at a fixed value of  $\epsilon$ . The estimated saturation values are marked in Fig. 3(b) by red dashed curves, which are still above the exponential curves given by Eq. (9). Thus, even after accounting for the finite-size effects, our numerical results are consistent with  $\epsilon_c = 0$ .

We check whether similar observations can also be made for the case of the PBC, whose results are shown in the lower panel of Fig. 3. Stronger finite-size corrections (which were suppressed by the exact particle-hole symmetry for the OBC with  $\alpha = \beta = 1/2$ ) are clearly visible in Fig. 3(d) in the form of  $J(0; L) > 1/4$ , which is in agreement with the exact result  $J(0; L) = \frac{1}{4(1-1/L)}$  for the PBC. Still, all observations made for the OBC can also be made for this case, as shown in Figs. 3(e) and (f). In particular, the exponential behavior of Eq. (9) again gives a good fit of  $\Delta_J$  for large values of  $\epsilon$ , which



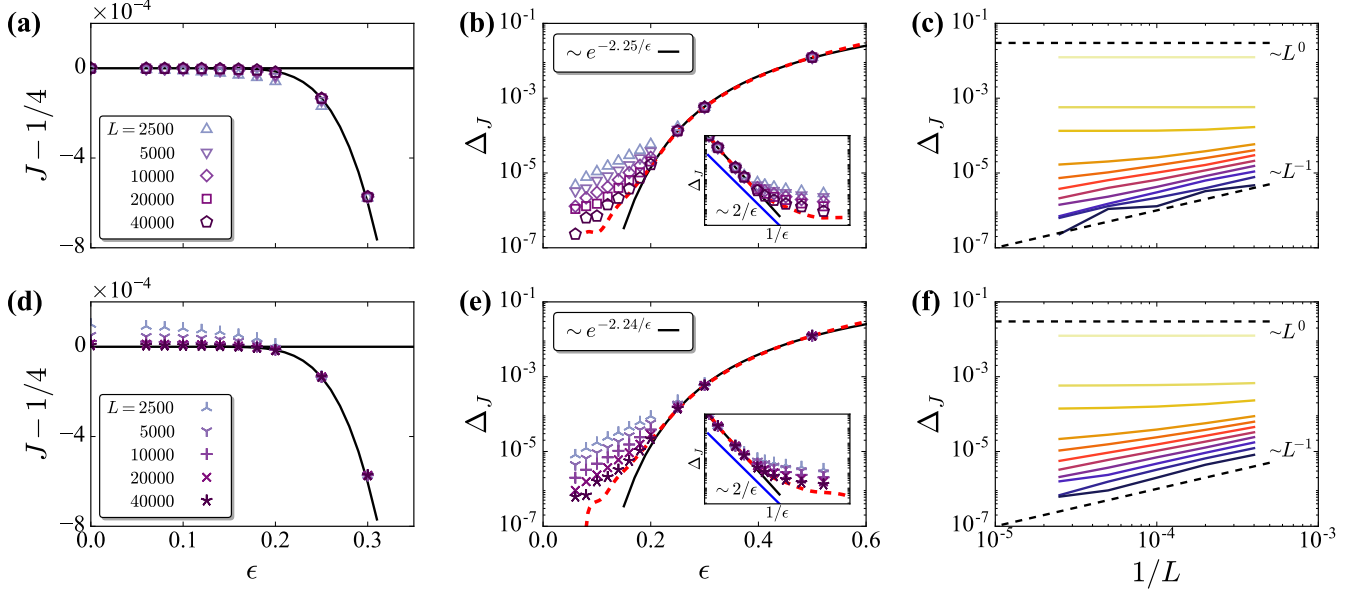


FIG. 3. The steady-state current  $J$  and the reduced current  $\Delta_J$  as the slow-bond strength  $\epsilon$  and the system size  $L$  are varied. (a) For the OBC, the symbols represent numerical data and the black solid lines represent the scaling form  $\Delta_J \sim \exp(-b/\epsilon)$ , with  $b$  estimated by curve fitting. (b) The same data and the scaling form are replotted in the new axes. The red dashed line indicates the estimated saturation values of  $\Delta_J$  when all finite- $L$  corrections decay as  $1/L$ . The blue solid line in the inset correspond to  $b \simeq 2$  proposed in the literature [17]. (c) The  $L$  dependence of  $\Delta_J$  is shown for  $\epsilon$  fixed at 0.06, 0.08, 0.1, 0.12, 0.14, 0.16, 0.18, 0.2, 0.25, 0.3, and 0.5 from bottom (darker colors) to top (lighter colors). (d-f) Similar plots are shown for the PBC.

gives an estimation  $b \simeq 2.25$ . The close agreement between the values of  $b$  estimated for these two different boundary conditions indicates an ensemble equivalence between closed and open systems.

In [20], a power-law behavior  $\Delta_b \sim |\epsilon - \epsilon_c|^\beta$  with  $\epsilon_c = 0.20(2)$  and  $\beta \simeq 1.46(4)$  was reported, which implies  $\Delta_J \sim |\epsilon - \epsilon_c|^{2\beta}$ . But our observations shown in Fig. 3, especially those for the OBC with  $\alpha = \beta = 1/2$  (the very boundary conditions used in [20]), do not support this behavior. In the following sections, we check whether similar observations can be made for different observables as well.

#### IV. PASSIVE SLIDER STATISTICS

As noted in Sec. II C, for  $\epsilon > \epsilon_c$  the average height profile of the BCSOS growth model develops a pair of tilted surfaces whose slopes are given by  $\Delta_b$ , so that the slow bond is located at the bottom of a valley (see Fig. 2). This implies that we may identify  $\epsilon_c$  by finding a measure which is sensitive to the slope. Thus passive sliders [27, 31–33], which are random walkers driven by the surface gradients without ever affecting the surface growth, provide a convenient tool for detecting slow-bond effects. In this section, we numerically study the statistics of two different types of passive sliders defined by [27], and discuss their implications on the slow-bond

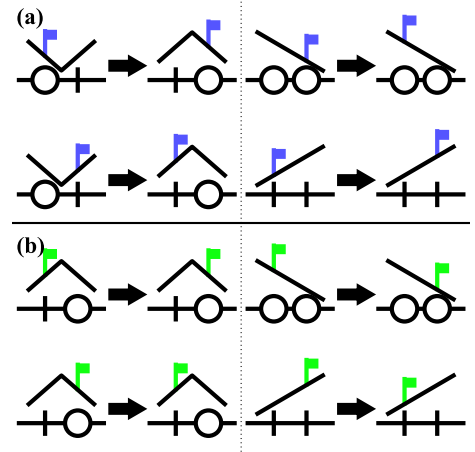


FIG. 4. All possible movements of passive sliders driven by the BCSOS growth model are shown for (a) positive sliders and (b) negative sliders.

problem. For the sake of brevity, and since we expect an ensemble equivalence for different boundary conditions (as implied by the results of Sec. III), here we restrict ourselves to systems with the OBC.

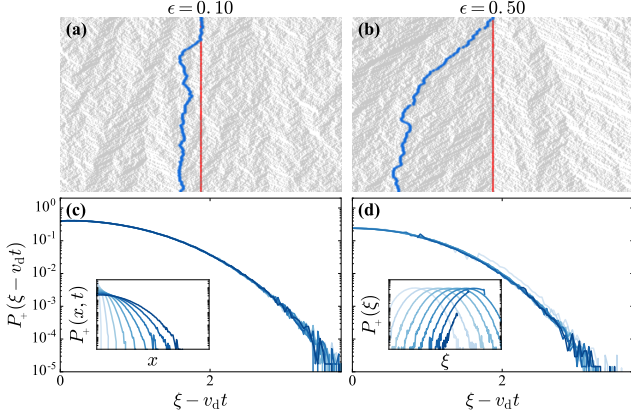


FIG. 5. Positive slider dynamics in the presence of a slow bond. (a, b) Slider trajectories (thick blue lines) starting from a fixed slow bond (thin red lines) at different  $\epsilon$ . The horizontal (vertical) direction represents space (time), with the time increasing in the downward direction. (c, d) Snapshots of the slider distribution for the rescaled position  $\xi \equiv xt^{-1/z_+}$  with the dynamic exponent  $z_+ = 3/2$ . The  $n$ -th snapshot is taken at  $t = 400n^2$ , where  $n = 1, \dots, 10$  (from lighter to darker colors). The drift velocity  $v_d$  is put equal to 0 for (c) and 0.223 for (d). The data are obtained over  $10^6$  samples using the OBC.

### A. Positive sliders

We first consider *positive sliders*, which are also called sliders performing *advection* within the context of fluid mechanics [27]. These sliders are driven uphill: for simplicity, we focus on the extreme case when only uphill movements are allowed in the middle of a slope. Randomness in direction arises only when the slider is next to the bottom of a valley, deciding on which slope to climb. Provided that the sliders and the surface evolve on a same time scale, we may define the coupled dynamics of positive sliders and the BCSOS surface growth as shown in Fig. 4(a), which shows all possible updates of the system.

The dynamics of positive sliders are analogous to those of second-class particles in the TASEP (see [5] for a review). It is well known that, in the maximal-current phase ( $\rho_b = 1/2$ ), the average position of the second-class particle remains stationary, while the width of the position evolves like  $\sigma_+(t) \sim t^{1/z_+}$ , with the dynamic exponent  $z_+$  given by the KPZ exponent  $3/2$ . On the other hand, in the low-density or high-density phase with nonzero  $\rho_b \neq 1/2$ , the average position of the second-class particle drifts at a velocity [34]

$$v_d = 1 - 2\rho_b, \quad (10)$$

while the width of the position distribution about this moving average spreads like  $\sigma_+(t) \sim t^{1/z_+}$ .

The behaviors of the second-class particles suggest that the distribution of positive sliders departing from the

slow bond satisfies the scaling form

$$P_+(x, t) = P_+(\xi - v_d t), \text{ where } \xi = xt^{-1/z_+}. \quad (11)$$

The drift velocity  $v_d$  becomes a function of the slow-bond strength  $\epsilon$ . Our numerical results confirm this scaling form (see Fig. 5). When the slow bond is weak ( $\epsilon = 0.1$ ), the distributions are collapsed by putting  $v_d = 0$ . When the slow bond is strong ( $\epsilon = 0.5$ ), a nonzero value of  $v_d$  has to be used. Despite these observations, without the knowledge of the exact value of  $\epsilon_c$ , we do not know for certain when  $v_d$  should be nonzero for Eq. (11) to be precise.

To study the effects of the slow bond more systematically, we observe how the mean and the root mean square of the slider position evolve in time. The results are shown in Fig. 6. We expect that the average position

$$\mu_+(t) \equiv \int dx x P_+(x, t) \quad (12)$$

asymptotically evolves like  $\mu_+ \sim t^{1/z_+}$  for  $\epsilon \leq \epsilon_c$  and  $\mu_+ \sim t$  for  $\epsilon > \epsilon_c$ . The curves in Fig. 6(a) show that for small values of  $\epsilon$  only the former behavior is observed, while for sufficiently large values of  $\epsilon$  the latter behavior starts to show up after some time.

This suggests the possibility of a crossover from anomalous diffusion to uphill translation. To make this crossover more visible, in Fig. 6(b) we plot the root mean square of the slider position defined by

$$\sigma_+(t) \equiv \left[ \int dx x^2 P_+(x, t) \right]^{1/2}, \quad (13)$$

which should satisfy  $\sigma_+ \sim t^{1/z_+}$  for  $\epsilon \leq \epsilon_c$  and  $\sigma_+ \sim t$  for  $\epsilon > \epsilon_c$ . It turns out that  $\sigma_+ t^{-1/z_+}$  initially decreases in time, but eventually starts to increase after some crossover time scale  $t_c$ , which seems to be a decreasing function of  $\epsilon$ .

As  $\epsilon$  is varied, we can identify  $t_c$  and the corresponding  $\sigma_+^* \equiv \sigma_+(t_c)$ , as shown in the inset of Fig. 6(b). This allows us to plot the crossover time  $t_c$  as a function of  $\epsilon$ , as shown in Figs. 6(c). The function is apparently exponential in  $1/\epsilon$ , in a manner very similar to Eq. (9) for  $\Delta_J$ . This suggests that  $t_c$  and  $\Delta_J$  are related by a scaling relation.

We note that the crossover time is inversely proportional to the drift velocity of the slider, i.e.,  $t_c \sim 1/v_d$ . From Eqs. (3), (6), and (10), we obtain a series of relations

$$v_d = -2\Delta_b \sim \Delta_J^{1/2}. \quad (14)$$

Combining these relations with Eq. (9) for  $\Delta_J$ , we obtain a relation between  $t_c$  and  $\epsilon$ :

$$t_c \sim \exp(b/2\epsilon), \quad (15)$$

whose form again suggests the possibility of an essential singularity at  $\epsilon_c = 0$  in a manner very similar to Eq. (9).

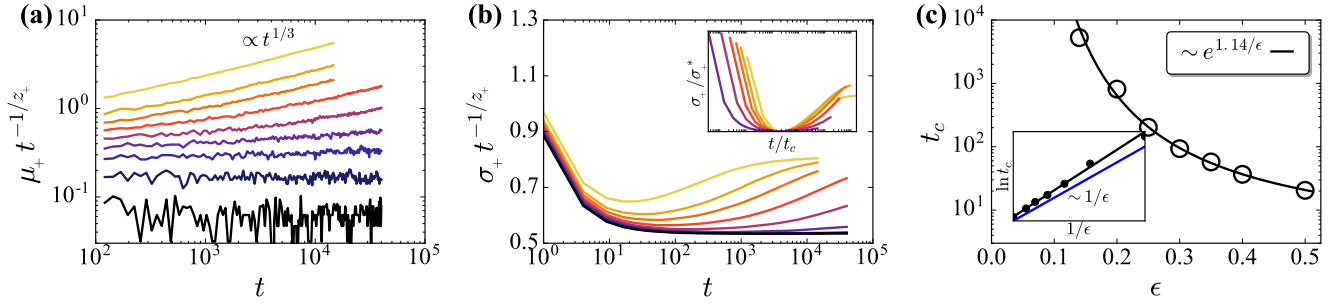


FIG. 6. Time evolutions of (a) the mean  $\mu_+$  and (b) the root mean square  $\sigma_+$  of the positive slider location for a system of size  $L = 10^4$  with the OBC. The dynamic exponent is given by  $z_+ = 3/2$ . The slow-bond strengths are given by  $\epsilon = 0, 0.06, 0.14, 0.2, 0.25, 0.3, 0.35, 0.4$ , and  $0.5$  from bottom (darker colors) to top (lighter colors). Based on the local minima of the curves in (b), we can plot (c) the crossover time  $t_c$  as a function of the slow-bond strength  $\epsilon$ , which shows an exponential dependence on  $1/\epsilon$  indicated by black curves. The blue line in the inset corresponds to the behavior proposed in the literature [17].

We fit our data for  $t_c$  to this relation (see Fig. 6(d)), which gives an estimation  $b \simeq 2.29$ . Since this is very close to the estimated values of  $b$  obtained in Sec. III, we can say that the statistics of positive sliders are consistent with those of the steady-state current  $J$ .

### B. Negative sliders

Now we consider *negative sliders*, also called sliders performing *anti-advection* in the fluid mechanical context [27]. In contrast to the positive sliders, these sliders are driven downhill. To simplify the model, we focus

on the case when only downhill movements are allowed in the middle of a slope, with randomness in direction arising only in the neighborhood of a hilltop, where the slider chooses which slope to roll down at random. If the sliders and the surface evolve on a same time scale, the coupled dynamics of negative sliders and the BCSOS surface growth can be defined as shown in Fig. 4(b).

Due to the inherent asymmetry of the KPZ dynamics, the statistics of negative sliders are quite different from those of positive sliders. While a negative slider on a KPZ surface without any global tilt (i.e., the maximal-current phase of TASEP) is known to exhibit an anomalous diffusion  $\Delta x \sim t^{-1/z_-}$ , no analytic prediction has been proposed for the dynamic exponent  $z_-$ ; there are only numerical estimations, which give an estimate  $z_- \simeq 1.75$  [35]. Our numerical results for small  $\epsilon$  seem to confirm this behavior; for  $\epsilon = 0.1$ , the distribution of the negative slider departing from the slow bond seems to satisfy the scaling form

$$P_-(x, t) = P_-(\xi), \text{ where } \xi = xt^{-1/z_-}, \quad (16)$$

with the dynamic exponent estimated as  $z_- \simeq 1.8$  (see Figs. 7(a) and (c)).

In contrast, when the slow bond is strong ( $\epsilon = 0.5$ ), the negative slider is trapped in the microscopic neighborhood of the slow bond, as shown in Fig. 7(b). This means that the distribution asymptotically behaves like

$$P_-(x, t) = P_-(x), \quad (17)$$

so that no rescaling with respect to time is required to collapse the distributions, as shown in Fig. 7(d). Since the exact value of  $\epsilon_c$  is unknown, we do not know for certain which of Eqs. (16) and (17) is the correct scaling form at a given value of  $\epsilon$  close to 0.

To obtain a more systematic view of the slow-bond effects, we observe how the root mean square of the slider

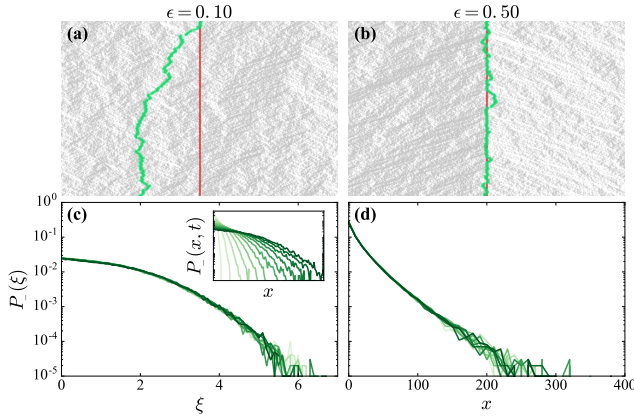


FIG. 7. Negative slider dynamics in the presence of a slow bond. (a, b) Sample slider trajectories (green fluctuating lines) originating from a slow bond (red straight lines) at different  $\epsilon$ . The horizontal (vertical) direction represents space (time), with the time increasing in the downward direction. (c, d) Snapshots of the slider distribution for the rescaled position  $\xi \equiv xt^{-1/z_-}$  with the dynamic exponent  $z_- \simeq 1.8$ . The  $n$ -th snapshot is taken at  $t = 1600n^2$ , where  $n = 1, \dots, 10$  (from lighter to darker colors). The data are obtained over  $5 \times 10^4$  samples using the OBC.

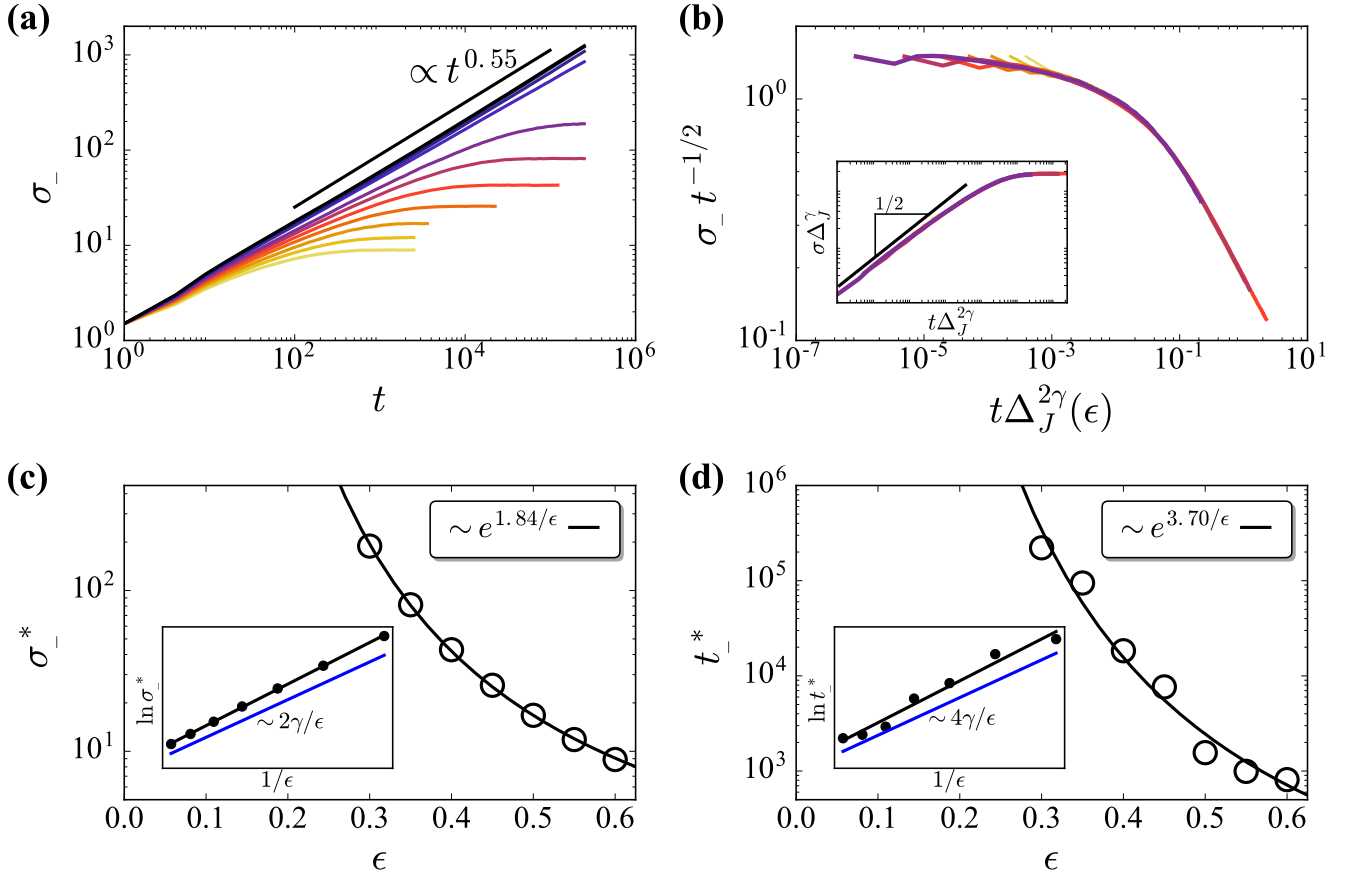


FIG. 8. Statistics of the negative slider distribution for a system of size  $L = 10^4$  with the OBC. (a) Time evolution of the width  $\sigma_-$  of the distribution, where the slow-bond strengths are given by  $\epsilon = 0, 0.06, 0.14, 0.2, 0.3, 0.35, 0.4, 0.45, 0.5, 0.55$ , and  $0.6$  from top (darker colors) to bottom (lighter colors). (b) Data collapse for some of the  $\sigma_-$  curves shown in (a), where  $\gamma = 0.833$ . (c) The width of the distribution at saturation and (d) the saturation time scale as functions of  $\epsilon$ . The black curves indicate exponential dependence on  $1/\epsilon$ , while the blue lines in the insets correspond to behaviors proposed in the literature [17].

TABLE I. Scaling relations between various observables and the slow-bond strength  $\epsilon$ . The scaling exponent  $\gamma \simeq 0.833$  is used. The parameter  $b$  governing the exponential dependence on  $1/\epsilon$  can be consistently estimated.

Observable	Scaling relation	$b$ (fitting)	Relative magnitude of $b$
Reduced current (OBC)	$\Delta_J \sim \exp(-b/\epsilon)$	2.25	1
Reduced current (PBC)	$\Delta_J \sim \exp(-b/\epsilon)$	2.24	1.00
Crossover time	$t_c \sim \Delta_J^{-1/2} \sim \exp(b/2\epsilon)$	2.29	1.02
Saturation width	$\sigma_-^* \sim \Delta_J^{-\gamma} \sim \exp(\gamma b/\epsilon)$	2.20	0.98
Saturation time	$t_-^* \sim \Delta_J^{-2\gamma} \sim \exp(2\gamma b/\epsilon)$	2.22	0.99

position defined by

$$\sigma_-(t) \equiv \left[ \int dx x^2 P_-(x, t) \right]^{1/2} \quad (18)$$

evolve in time, which is shown in Fig. 8(a). Our results suggest that the width of the slider distribution saturates to  $\sigma_-^*$  beyond some saturation time scale  $t_-^*$ , with both  $\sigma_-^*$  and  $t_-^*$  decreasing as functions of  $\epsilon$ . Interestingly,

these quantities seems to satisfy a scaling relation

$$t_-^* \sim (\sigma_-^*)^2, \quad (19)$$

which implies that there is some normal diffusion involved. We also expect that  $\sigma_-^*$  and  $t_-^*$  are related to the reduced current  $\Delta_J$ , which indicates the global influence of the slow bond. Thus we can assume the scaling



relations

$$\sigma_-^* \sim \Delta_J^{-\gamma}, \quad t_-^* \sim \Delta_J^{-2\gamma}, \quad (20)$$

which suggests a scaling ansatz

$$\sigma_-(t, \Delta_J) = \Delta_J^{-\gamma} \Psi(t \Delta_J^{2\gamma}) = t^{1/2} \Phi(t \Delta_J^{2\gamma}). \quad (21)$$

From our numerical results, we obtain  $\gamma \simeq 0.833$ , as shown in Fig. 8(b) and its inset. Combining Eq. (20) with Eq. (9) for the exponential dependence of  $\Delta_J$ , we can show that  $\sigma_-^*$  and  $t_-^*$  exhibit similar exponential behaviors, which are stated in Table I and confirmed by numerics in Figs. 8(c) and (d). The values of the parameter  $b$  estimated from these results seem consistent with those obtained in the previous sections.

## V. SUMMARY

Based on numerical observations of the steady-state current and the dynamics of passive sliders, we studied how strong a slow bond should be to affect the macroscopic properties of systems belonging to the KPZ universality class. Irrespective of boundary conditions (both

PBC and OBC) and observables (see Tab. I to check their mutual consistency), our results were largely consistent with an essential singularity at  $\epsilon_c = 0$  proposed by [17]. Although this is not a definite proof of  $\epsilon_c = 0$ , we conclude that the critical behaviors near  $\epsilon_c = 0.20(2)$  reported in [20] are artifacts due to the finite size of the system: even if  $\epsilon_c$  is nonzero, it must be smaller than the value estimated by [20]. This also suggests that other numerical results [21, 22] claiming  $\epsilon_c > 0$  are subject to similar artifacts.

Statistics of negative sliders considered in our study leave some open questions. The scaling relations of Eqs. (19) and (20) remain pure observations without analytical arguments explaining them. Identifying the possible origin of these behaviors and deriving the nontrivial exponent  $\gamma$  could be interesting subjects for future works.

## ACKNOWLEDGMENTS

This work was supported by the National Research Foundation of Korea (NRF) funded by Korean government [Grants No. NRF-2014R1A1A40103864 (H.S., M.H.) and NRF-20110028908 (H.S., H.J.)]. Y.B. was supported in part at the Technion by a fellowship from the Lady Davis Foundation.

- 
- [1] M. Kardar, G. Parisi, and Y.-C. Zhang, *Phys. Rev. Lett.* **56**, 889 (1986).
  - [2] A.-L. Barabási and H. E. Stanley, *Fractal Concepts in Surface Growth* (Cambridge, 1995).
  - [3] T. Halpin-Healy and Y.-C. Zhang, *Phys. Rep.* **254**, 215 (1995).
  - [4] J. Krug, *Adv. Phys.* **46**, 139 (1997).
  - [5] R. A. Blythe and M. R. Evans, *J. Phys. A* **40**, R333 (2007).
  - [6] M. Kardar and Y.-C. Zhang, *Phys. Rev. Lett.* **58**, 2087 (1987).
  - [7] I. Corwin, *Rand. Mat.* **01**, 1130001 (2012).
  - [8] J. Quastel and H. Spohn, *J. Stat. Phys.* **160**, 965 (2015).
  - [9] K. A. Takeuchi and M. Sano, *Phys. Rev. Lett.* **104**, 230601 (2010); K. A. Takeuchi, M. Sano, T. Sasamoto, and H. Spohn, *Sci. Rep.* **1**, 34 (2011), article.
  - [10] H. Spohn, *J. Phys. A* **16**, 4275 (1983).
  - [11] P. L. Garrido, J. L. Lebowitz, C. Maes, and H. Spohn, *Phys. Rev. A* **42**, 1954 (1990).
  - [12] J. R. Dorfman, T. R. Kirkpatrick, and J. V. Sengers, *Ann. Rev. Phys. Chem.* **45**, 213 (1994).
  - [13] The slow-bond problem can also be posed in the context of condensation transitions; see E. N. M. Cirillo, M. Colangeli, and A. Muntean, *Phys. Rev. E* **94**, 042116 (2016).
  - [14] S. A. Janowsky and J. L. Lebowitz, *Phys. Rev. A* **45**, 618 (1992).
  - [15] A. B. Kolomeisky, *J. Phys. A* **31**, 1153 (1998).
  - [16] S. A. Janowsky and J. L. Lebowitz, *J. Stat. Phys.* **77**, 35 (1994).
  - [17] O. Costin, J. L. Lebowitz, E. R. Speer, and A. Troiani, *Bull. Inst. Math., Acad. Sin. (New Series)* **8**, 49 (2013).
  - [18] L.-H. Tang and I. F. Lyuksyutov, *Phys. Rev. Lett.* **71**, 2745 (1993).
  - [19] L. Balents and M. Kardar, *Phys. Rev. B* **49**, 13030 (1994); H. Kinzelbach and M. Lässig, *J. Phys. A* **28**, 6535 (1995); T. Hwa and T. Nattermann, *Phys. Rev. B* **51**, 455 (1995); E. B. Kolomeisky and J. P. Straley, *Phys. Rev. B* **51**, 8030 (1995); M. Lässig, *J. Phys.: Cond. Matter* **10**, 9905 (1998).
  - [20] M. Ha, J. Timonen, and M. den Nijs, *Phys. Rev. E* **68**, 056122 (2003).
  - [21] D. Kandel and D. Mukamel, *Europhys. Lett.* **20**, 325 (1992).
  - [22] J. H. Lee and J. M. Kim, *Phys. Rev. E* **79**, 051127 (2009).
  - [23] M. Myllys, J. Maunukela, J. Merikoski, J. Timonen, V. K. Horváth, M. Ha, and M. den Nijs, *Phys. Rev. E* **68**, 051103 (2003).
  - [24] We note that, when the updates are parallel, the TASEP with a slow bond was analytically solved, yielding  $\epsilon_c = 0$  [36].
  - [25] R. Basu, V. Sidoravicius, and A. Sly, ArXiv e-prints (2014), arXiv:1408.3464 [math.PR].
  - [26] J. Schmidt, V. Popkov, and A. Schadschneider, *Europhys. Lett.* **110**, 20008 (2015).
  - [27] B. Drossel and M. Kardar, *Phys. Rev. B* **66**, 195414 (2002).
  - [28] H. van Beijeren, *Phys. Rev. Lett.* **38**, 993 (1977).
  - [29] Here the Mersenne Twister is used as a pseudo-random number generator, which is one of the most widely used. See <http://www.math.sci.hiroshima-u.ac.jp/~m-mat/MT/ARTICLES/earticles.html>.

- [30] Due to the exact particle-hole symmetry, in this case  $J(0; L) = 1/4$  holds for any  $L$ .
- [31] C.-S. Chin, [Phys. Rev. E \*\*66\*\*, 021104 \(2002\)](#).
- [32] A. Nagar, *Steady States of Passive Particles Sliding on Fluctuating Surfaces*, Ph.D. thesis, Tata Institute of Fundamental Research Mumbai (2006).
- [33] A. Nagar, S. N. Majumdar, and M. Barma, [Phys. Rev. E \*\*74\*\*, 021124 \(2006\)](#).
- [34] This velocity is equal to the *group velocity*, which is the velocity at which density envelopes travel.
- [35] While [27] claims that  $z_-$  varies continuously according to the model details (reporting various values between 1.74 and 1.98), [32] claims that a universal value  $z_- \simeq 1.75$  describes the true asymptotic behavior.
- [36] G. Schütz, [J. Stat. Phys. \*\*71\*\*, 471 \(1993\)](#); [Phys. Rev. E \*\*47\*\*, 4265 \(1993\)](#); B. Scoppola, C. Lancia, and R. Mariani, [J. Stat. Phys. \*\*161\*\*, 843 \(2015\)](#).